(Received 30 May 2024, Accepted 25 August 2024, Scheduled 8 September 2024)

Nonlinear Microwave Device LabVIEW Automatic Test Bench: Double-Frequency IMD3 Characterization

Xin Cheng[1], Fayu Wan[1,*], Vladimir Mordachev[2], Eugene Sinkevich[2], Xiaohe Chen[3], and Blaise Ravelo[1]

[1]*Nanjing University of Information Science & Technology (NUIST), Nanjing 210044, Jiangsu, China*
[2]*Belarusian State University of Informatics and Radioelectronics, Minsk, Belarus*
[3]*China University of Petroleum, College of Information Science and Engineering, Beijing, China*

ABSTRACT: The active component nonlinear (NL) effect causes undesirable RF and microwave system electromagnetic interference (EMI) problems which penalizes the communication system performance by signal distortion. Therefore, a relevant NL component measurement method is needed to predict the transceiver system EMI effect. However, the NL measurement characterization of RF and microwave active devices remains a fastidious and time cost task. An innovative NL test bench automatized by LabVIEW®control interface is featured in this research work. The design technique of the NL test methodology is described. The developed automatic test bench is tested with a microwave power amplifier (PA) operating at 2.4 GHz based on double-frequency (DF) method. The experimental test setup including the LabVIEW®test control parametrization and data acquisition is described. The test bench effectiveness was assessed by the third-order intermodulation (IMD3) PA measurement with DF method. The theoretically calculated and measured IMD3 amplitudes based on DF input signal are in very good correlation. Thanks to its advantages in terms of simplicity, flexibility, and time cost, the innovative NL automatic test bench is very useful for transceiver system EMI analyses.

1. INTRODUCTION

The future mobile communication system intends to operate by respecting electromagnetic interference (EMI) compliances by meeting 6G technology requirements [1]. Different technical challenges are expected with the critical saturation of operating frequency bands in addition to the electronic equipment density [1–3]. Furthermore, due to the design complexity and environment electromagnetic (EM) pollution, the 5G Internet-of-Things (IoT) [2] and 6G [3] system designers must overcome the EM compatibility (EMC) challenges. The susceptibility of electronic communication systems to interact with complex EM environment becomes critical and requires relevant EMC investigation [4, 5]. For 6G transceiver (TxRx), the EMC and EMI design [3] constitutes a real breakthrough for communication system industries.

Research works on EMI investigation related to microwave systems and components are still going on to minimize the drastic effect on communication quality. For example, the use of high-power transmitter (Tx) [6] increases the risk of broadband communication EMI over sensitive electronic devices due to nonlinear (NL) effect [7]. In addition to intense EM radiation, the electronic communication performance may suffer from NL signal distortion [8, 9]. All these factors require relevant EMI analysis methods for both receiver (Rx) and Tx systems [10–13]. Moreover, more and more attention of EMC design researchers has been paid to RF/microwave NL characterization topic [14–16]. The NL microwave circuit characterization gains more and more importance [17–24]. Multi-tone signal tests are particularly useful for TxRx communication system EMI assessment due to NL circuit characterization [25]. Some analysis methods [26–30] for more general circuits such as the widely used harmonic balance [26] and Volterra series analysis ones [27, 28] to solve weak NL circuits have been developed to solve different NL circuits. A large number of parasitic responses, including desensitization, blocking, spurious response, high-order intermodulation (IM), cross modulation, and other complex NL effects have been identified for power amplifiers (PAs) under the common excitation of a variety of EMI signals [31, 32]. Nonlinearity (NLT) affects the normal operation of the receiving system by performance degradation [33, 34]. Therefore, accurate NL characteristic measurement of microwave devices as PA [5, 7, 11–13] is needed to deal with EMI undesirable effects.

To analyze the EMI effect from communication modulated signal distortion caused by IM, double-frequency (DF) test method was approved as the most efficient one [11, 24, 32, 35–37]. DF method consists in injecting two or more controllable harmonic signals into the NL device under test (DUT) [36]. The analysis and processing of DF measurement results enable the assessment of NL characteristics as third-order IM distortion (IMD3). Nevertheless, DF experimental tests are particularly fastidious and time-consuming for RF/microwave measurement engineers [11, 24, 32, 35–37]. A relevant method enabling the control of measurement instrument and also acquiring the NL characteristics of the power DUT is still needed. A collect method must integrate the measurement data repre-

* Corresponding author: Fayu Wan (fayu.wan@nuist.edu.cn).

senting the input and output signal parameters. In this way, the present research work contributes originally to the development of DF test bench enabling the evaluation of the TxRx EMI from cross modulation.

The present paper is divided into five sections as follows:

- First, Section 2 explains the methodological investigation on the automatic test bench of microwave NL active devices. The basic theoretical approach is reminded in order to highlight the DF method fundamental functionality.
- Section 3 explains the emulation of the different modules developed to control the innovative automatic NL device test bench. The schematic diagrams representing the different input and output interfaces designed with LabVIEW®virtual measurement instrument platform are described.
- Section 4 focuses on the testability study of the innovative NL characterization automatic platform. As proof of concept (POC), NL characterization uses a Gallium Nitride (GaN) PA as DUT elaborated by DF method. The NL experimentation will explore the IMD3 measurement test versus input signal frequency and power.
- Section 5 discusses the innovative automatic test bench with different cases of DF input parametrization. The two cases of same and different amplitude inputs are considered. The main advantages of the developed test bench are also described.
- Last, Section 6 provides the final conclusion.

2. MICROWAVE DEVICE NL AUTOMATIC TEST METHODOLOGY

The present section introduces the theoretical methodology of the innovative automatic test bench intended for the microwave device NL characterization.

2.1. Single-Frequency Harmonic Theoretical Analysis of Two-Port NL System Response

Figure 1 represents the two-port block diagram of NL network transfer function. If the network is memoryless, the output can be expressed as a power series of the t-time dependent input signal v_i [13, 25, 37]:

$$v_o(t) = \sum_{m=1}^{n} k_m v_i^m(t) \tag{1}$$

where n is theoretically equal to infinity.

FIGURE 1. Two-port NL network.

By assuming single tone input $v_i(t) = A\cos(\omega_0 t)$ of carrier $f_0 = \omega_0/(2\pi)$, for linear networks $k_i = 0$ if $i > 1$, the weak NL network as the case of the present study is limited to low order harmonics with $n = 3$. Therefore, after linearization, Equation (1) becomes:

$$v_o(t) \approx V_{o0} + V_{o1}\cos(\omega_0 t) + V_{o2}\cos(2\omega_0 t) + V_{o3}\cos(3\omega_0 t) \tag{2}$$

where the harmonic amplitudes are defined by:

$$\begin{cases} V_{o0} = \dfrac{k_2 A^2}{2} \\ V_{o1} = k_1 A + \dfrac{k_3 A^3}{4} \\ V_{o2} = \dfrac{k_2 A^2}{2} \\ V_{o3} = \dfrac{3k_3 A^3}{4} \end{cases}. \tag{3}$$

For the case of DF harmonic input, we have IMD3 expressed in the following subsection.

2.2. Theory on NL IMD3 Component with DF Harmonic Input Method

For a basic understanding of the DF method, a theoretical approach is reminded in this subsection. Accordingly, let us consider the case of two-tone (TT) excitation harmonic signal:

$$v_i(t) = A_1\cos(\omega_1 t) + A_2\cos(\omega_2 t) \tag{4}$$

under condition:

$$\Delta f_{12} = |f_2 - f_1| = \frac{|\omega_2 - \omega_1|}{2\pi} << f_0 = \frac{\omega_0}{2\pi}. \tag{5}$$

After substituting Equation (4) into Equation (1) for $n = 3$, the NL output expression in the working frequency band around f_1 and f_2 can be rewritten as:

$$v_o(t) \approx \begin{Bmatrix} k_2(A_1^2 + A_2^2)/2 + k_1 A_1\cos(\omega_1 t) \\ + k_1 A_2\cos(\omega_2 t) \\ + k_2 A_1 A_2\left[\cos(\omega_2 - \omega_1)t\right] + k_3 A_1/4 \\ \left[3(A_1^2 + 2A_2^2)\cos(\omega_1 t)\right] + k_3 A_2/4 \\ \left[3(A_2^2 + 2A_1^2)\cos(\omega_2 t)\right] + 3k_3 A_1 A_2/4 \\ \left[A_1\cos(2\omega_1 - \omega_2)t + A_2\cos(2\omega_2 - \omega_1)t\right] \end{Bmatrix}. \tag{6}$$

For the case where $A_1 = A_2 = A$, the previous NL output expression can be rewritten as:

$$v_o(t) \approx \begin{Bmatrix} k_2 A^2 + k_1 A\left[\cos(\omega_1 t) + \cos(\omega_2 t)\right] + \\ k_2 A^2\left[\cos(\omega_1 - \omega_2)t\right] \\ + A(k_1 + 9k_3 A^2/4)\left[\cos(\omega_1 t) + \cos(\omega_2 t)\right] + \\ 3k_3 A^3/4\left[\cos((2\omega_2 - \omega_1)t + \cos((2\omega_1 - \omega_2)t)\right] \end{Bmatrix}. \tag{7}$$

From the above analysis, it can be seen that when the excitation signal is a DF excitation signal, the output of the NL network generates a series of combined frequency components in addition to the fundamental wave and DC components, namely:

$$\omega_{m,n} = m\,\omega_1 + n\,\omega_2 \tag{8}$$

where m, $n = \{-1, 0, 1, 2\}$, and the $m + n$ sum is the order of the combined frequency $\omega_{m,n}$. Whether it is a weak NL circuit or a strong NL circuit, when the input of the circuit is coupled with the excitation signal, a series of combined frequency components of the excitation signal frequency will be generated at the output end, which is the basis for judging the NL circuit. The PA contains a semiconductor device with NL characteristics, such as triode, and when these devices work in the NL region or saturation region, the output voltage will show limiting characteristics, so that the circuit composed of these devices will produce NLT. Therefore, when a DF signal is input, due to the existence of NLT, in addition to the fundamental wave, the output of the PA also generates a series of frequency combination components [13, 37], which are the interference components in the output response of the PA.

2.3. Synoptic Diagram Description of NL Test

The developed NL test bench of PA as DUT operates according to the synoptic diagram is depicted by Fig. 2. During the test, the PA is fed through the constituting field effect transistor (FET) gate and gain by two DC power supplies denoted by DC-PS_1 and DC-PS_2, respectively.

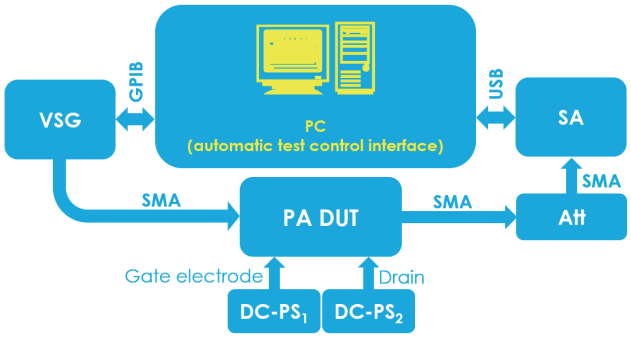

FIGURE 2. Synoptic diagram of developed PA NL test bench.

The interface implemented on the personal computer (PC) to control the NL test constitutes the innovative module of the test bench. The PC interface systematically drives the VSG and spectrum analyzer (SA) through an attenuator (Att) in order to save the input and output signals automatically. The vector signal generator (VSG) provides the input signals inputted to the PA. The original design of automatic control is described in the following section.

3. DESCRIPTION OF THE INNOVATIVE LABVIEW®INTERFACE BASED AUTOMATIC TEST BENCH FOR NL MICROWAVE DEVICES

The design method of the control panel interfacing and driving the innovative automatic NL test bench is developed in this section.

3.1. General Description

The DF automatic test model used in this paper is aimed to test the different interval frequencies of the TT signal at a single frequency point (such as 2.4 GHz or 2.5 GHz). The VSG provides directly the tri-tone signals. The interface control driving the tri-frequency NL test system developed in this paper is based on the idea of LabVIEW virtual instrument or graphic program. The host PC serves for design and development. The complete test system is composed of standard measurement and control bus, hoping to have good scalability, ease of use, maintainability, reliability, and security. According to the above requirements, the main functions of the LabVIEW interface are:

- Automatic system initialization/calibration;
- Generation of DF graph;
- Recording, display, and storage of test data;
- Based on the scalability of the DF automatic test system, the DF automatic test system can be extended to be used for multi-frequency test.

The developed original test bench enables technical support for studying the NL effect influence of transceiver multi-carrier on power devices and systems in complex EM environments.

3.2. Instrument Control Module

The control of the NL test instrument introduced in Fig. 2 by the controlling computer is realized based on standard commands for programmable instruments (SCPI).

The PC emulates and compiles each function module of the NL test bench operation in series. Then, the designed driver interface of the NL test bench completes the overall command of the system work by sending and receiving operating signal data to each module. The VSG providing the input signals and SA dedicated to visualize the measured signal spectra are selected as test instruments. During the test, they communicate to the PC by GPIB acquisition card and USB data line, respectively. In the system initialization stage, the PC controls the VSG and SA for frequency setting, power setting, and other operations, as indicated in the schematics displayed by Fig. 3(a) and Fig. 4(b), respectively. Considering practicality and esthetics, a graphical interface is designed on the front panel of LabVIEW for both VSG and SA control. The executable front panel of the automatic NL test bench is schematized in Fig. 4.

Behind the previous interface, specific commands are also designed for reading and saving data module as described in the following subsection.

3.3. Read and Save Data Module

After connection of the DUT as illustrated by the synoptic depicted by Fig. 2, the NL measurement operates when the instruments VSG, SA, and driver PC constituting the test bench are running and activated in ON-mode. The LabVIEW schematic diagram shown in Fig. 5(a) represents the graphic program for parametrizing the latency corresponding to the time duration to stabilize and visualize the measured signals. The NL test

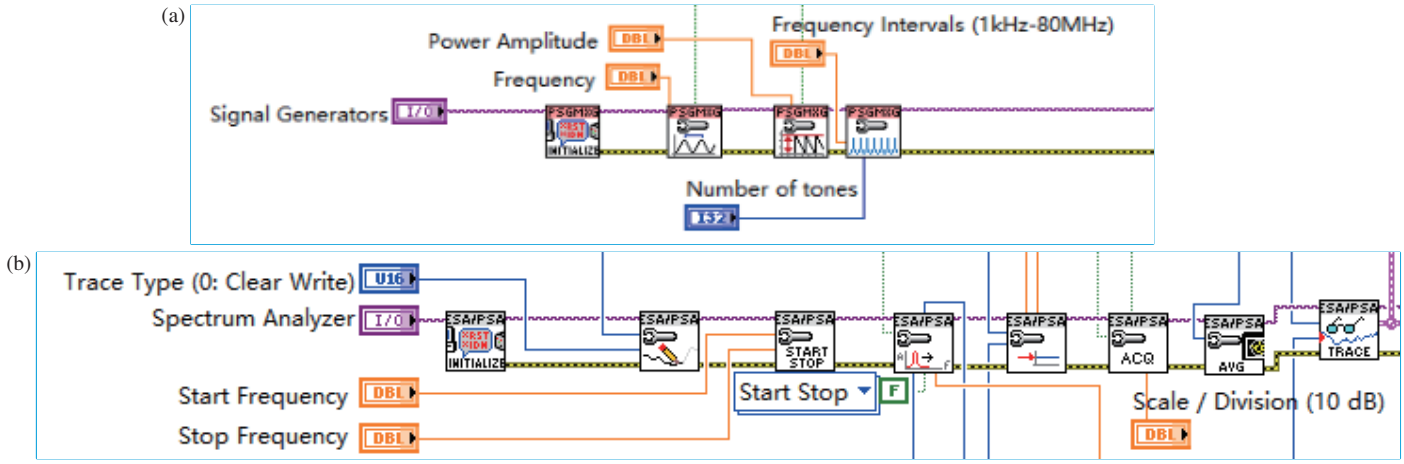

FIGURE 3. LabVIEW schematic diagrams for (a) VSG and (b) SA control.

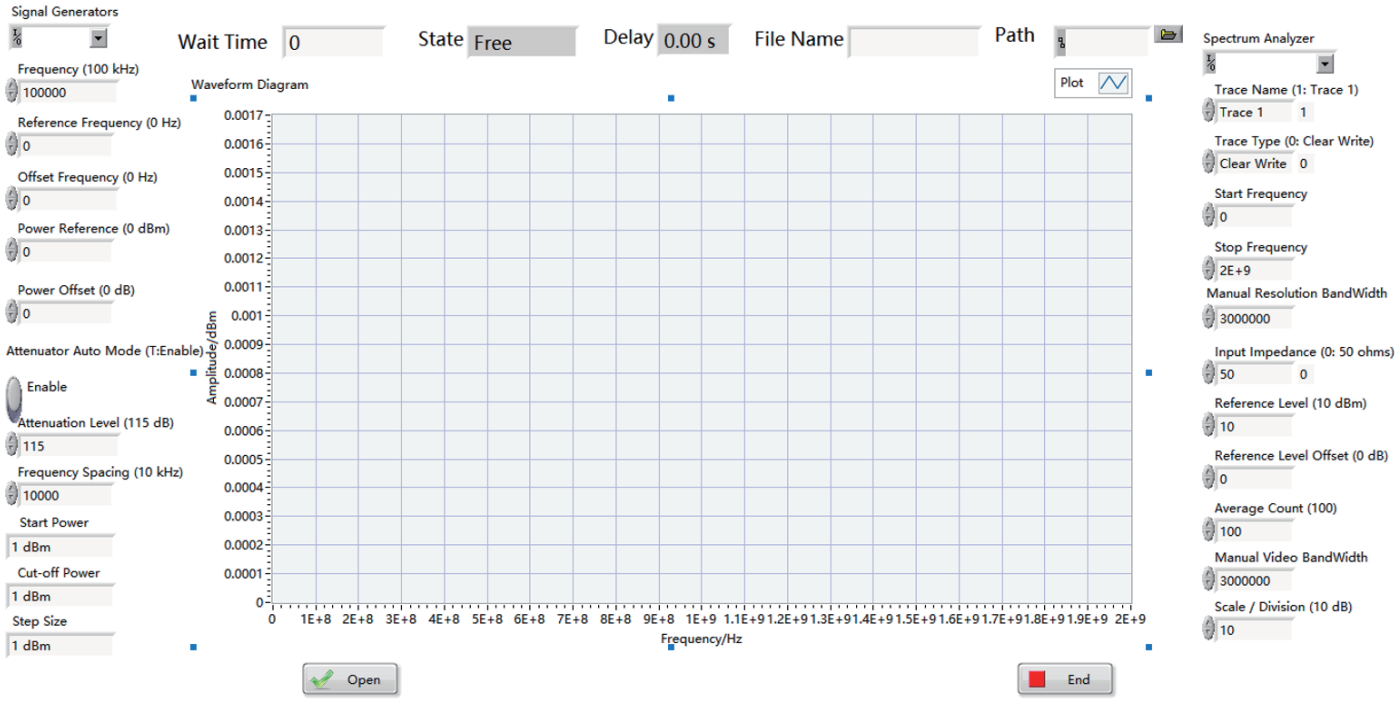

FIGURE 4. LabVIEW interface of the developed NL test bed.

achievement must be fulfilled by data reading/saving. The configuration module dedicated to that task is highlighted by the LabVIEW schematic diagram as displayed in Fig. 5(b), respectively. The main operation objective during the test is to automatically measure the input and output communication signal spectra by paying attention to the signal amplitudes or power at the specific test frequencies.

During the test process, the main actions are:

- Action 1: The PC interface controls the used instruments.
- Action 2: The NL measurement result visualization is achieved after consideration of specific delay to set the measured signal spectra. The delay must correspond to a period of time to wait for the signal to stabilize.
- Action 3: The LabVIEW driver reads and saves the operation data representing the input and output power versus frequency and the test sample sequences.
- Action 4: Afterwards, all the data is directly saved as a CSV file according to the input and output signal amplitudes which are represented by powers versus frequencies.

The practical operability of the developed NL automatic test bench is approved in the following section.

4. POC OF GAN PA DESCRIPTION AND SINGLE-FREQUENCY NL CHARACTERIZATION

As POC of the automatic test bench, the NL measurement results of the active microwave device represented by a PA with

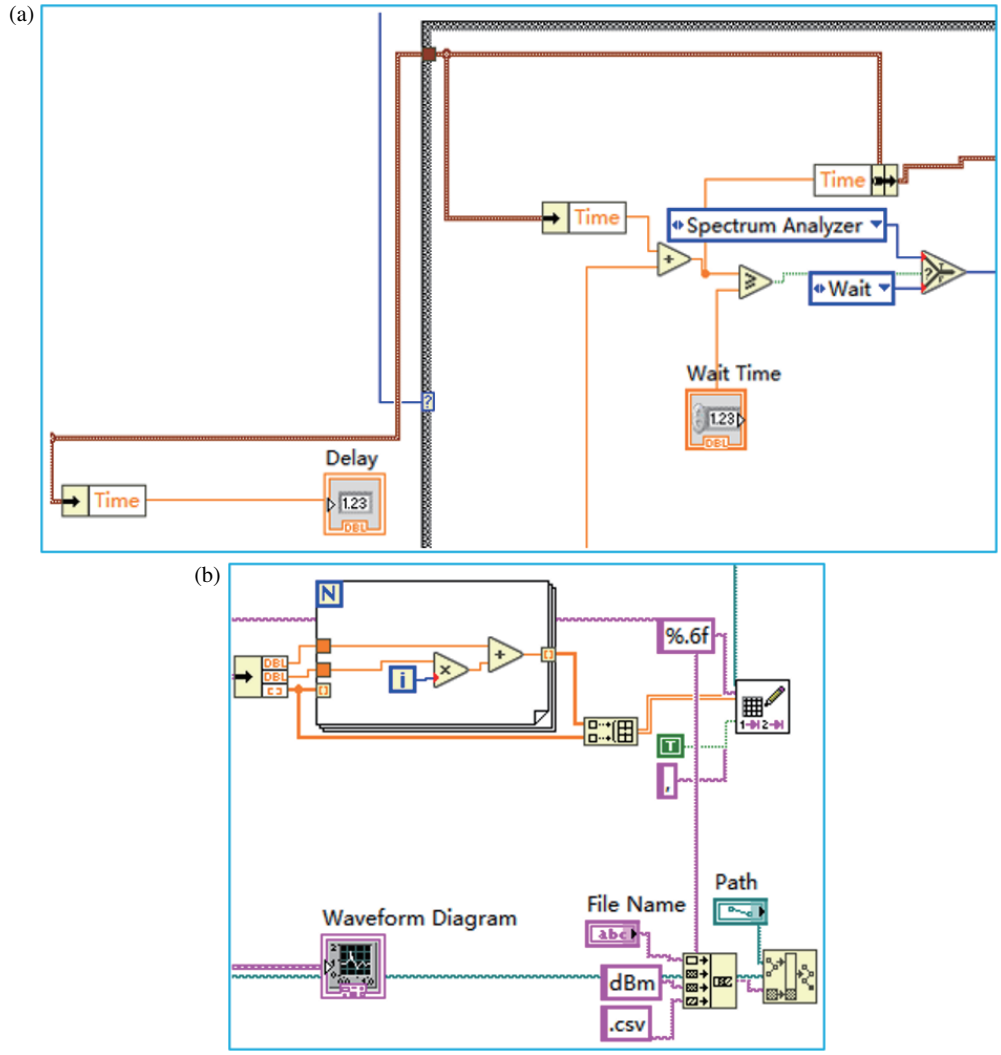

FIGURE 5. (a) Time delay and (b) read/save data module LabVIEW diagram.

the previously designed test bed are examined in the present section.

4.1. Choice of the POC Test Frequency Band

As POC of the performed experimental operation test, the working frequency band was the ISM standard frequency band which refers to most popular worldwide wireless communication. The considered standard frequency band centered by $f_0 = 2.4\,\text{GHz}$ is largely used in household and commercial fields, for example, with Bluetooth®technology. To guarantee the data communication quality in this working frequency band, it is interesting to analyze the EMI related to the microwave active component NLT. Therefore, a stronger anti-interference ability must be ensured during the design phase of electronic products. The GaN PA DUT investigated in the present section is designed and implemented in our laboratory. The considered GaN PA has nominal gain $Gain(f_0) = 38\,\text{dB}$ and is susceptible to operation in the frequency band between 2 GHz and 6 GHz locally. Fig. 6 represents a photograph of the PA DUT.

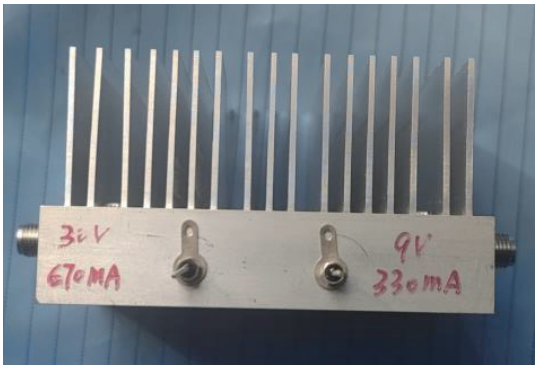

FIGURE 6. Photograph of the PA DUT.

The experimental setup of the automatic NL test bench with the PA DUT is described in the following subsection.

4.2. Description of Experimental Setup

The suitable instruments necessary for the experimental setup proposed in the diagram shown in Fig. 2 were chosen to set

the NL test bed. The used principal equipment includes Agilent E8267D VSG, GaN PA as DUT, with attenuation value of 20 dB Att referenced by 2.92TS20-20-40, Agilent E4447A spectrometer, Agilent E3632A DC PS_1, Agilent E3648A DC PS_2, and several coaxial lines and adapters. Table 1 indicates the technical specifications of each instrument employed during the NL test measurement.

TABLE 1. Specifications of employed instruments for the automatic NL test bed.

Designation	References	Specification
PC	ThinkPad	Equipped Windows 10 OS and with LabVIEW 20
VSG	Agilent E8267D	250 kHz-44 GHz
SA	Agilent E4447A	3 Hz–42.98 GHz
DC PS	Agilent E3648A	0–8 V, 5 A/0–20 V, 2.5 A
	Agilent E3632A	0–15 V, 5 A/0–30 V, 4 A
Attenuator	2.92TS20-20-40	20 dB

A photograph of the overall test bed including all the employed instruments and the LabVIEW control interface PC is displayed by Fig. 7. To validate the operability of the NL automatic test bed, several experiments with single and double tone signals with the PA DUT were performed. To do this, the following steps were followed:

- First, check the instruments installation and connection.
- Then, the delay time must take into account some measurement test factors such as the instruments' reaction speed generally between 3 and 5 seconds.
- After the waiting time, the file name and save path are configured, and click Start collection,
- Finally, after completing collection, click Stop button to complete a test.

The NL test results with single carrier frequency is discussed in the following subsection.

4.3. PA Power Series Coefficient Extraction from Single Carrier Frequency NL Test

To carry out the single tone signal experimentation, the VSG output was adjusted in the front panel of LabVIEW as seen in Fig. 5 to f_0-carrier frequency and the input signal amplitude $P_{in} = 0$ dBm. The SA screenshot representing the PA output signal spectrum obtained through the automatic NL test bed with single carrier input signal f_0 is viewed in Fig. 8. The visualized output with 5-GHz center frequency and 6-GHz span takes into account the SA protection 20-dB attenuator.

One can observe the NL effect witnessed by the apparition of fundamental frequency f_0 and the corresponding two harmonics in this spectral plot. Table 2 indicates the values of these spectral rays of output power frequency position and level $P_{out}(f_0, 2f_0, 3f_0)$.

In fact, the PA NL coefficients were extracted from single frequency spectrum plotted by Fig. 9 by means of fundamental and harmonic output magnitudes $V_{o,m} = \{1, 2, 3\}$ defined in Equation (2). By denoting $R_0 = 50\,\Omega$ the SA input impedance and associated voltage magnitudes are calculated from relationship:

$$V_{o,m} = \sqrt{10^{\frac{P_{out,dB}(m\,f_0)}{10}} R_0} \tag{9}$$

with $R_0 = 50\,\Omega$. It should be underlined that because of the SA frequency band limitation, it is more convenient to consider V_{o2} to determine k_2. The NLT coefficients of the DUT PA can be determined by inverting the amplitudes of harmonic by means of Equation (3):

$$\begin{cases} k_1 = \dfrac{3V_{o1} - V_{o3}}{3A} \\ k_2 = \dfrac{2V_{o2}}{A^2} \\ k_3 = \dfrac{4V_{o3}}{3A^3} \end{cases}. \tag{10}$$

Further DF NL characterization from the developed automatic test bed is explored in the following sections.

5. ANALYSES OF IMD3 MEASUREMENT VERSUS FREQUENCY, INPUT AND OUTPUT POWER AMPLITUDES

The automatic results of IMD3 NL test are characterized in this section based on the previously described POC. The characterization test enables the segregation of zones of weak and strong NL regions versus the input signal power level. Two different categories of test were performed with fixed and variable amplitudes of harmonic components v_1 and v_2 constituting input signal v_i.

5.1. PA Output Spectral Characterization with DF Experimentation

To validate the DF operability of the original NL test bed, further experimentation was performed. During the DF test, the input test signal power was gradually and automatically increased from $P_{in,\min} = -20$ dBm to $P_{in,\max} = 10$ dBm at an interval of $\Delta P_{in} = 2$ dBm, and the frequency interval of the TT signal was fixed to $\Delta f_{12} = 10$ MHz. The obtained result data is read through the automatic control interface. The PA input signal is extracted to subtract the long coaxial line loss of the VSG. The PA RF output signal power is the attenuation value of the measured peak power superimposed short coaxial line and the attenuator.

The cartographies of output signal spectra obtained through NL testing with DF input signals with frequencies $f_1 = 2.395$ GHz and $f_2 = 2.405$ GHz are shown in Fig. 9.

It is worth to emphasize from the spectrum mapped in Fig. 9(a) that there is a small signal around f_0 for the DF signal. The unexpected effect is caused by the impurity of the VSG output. The observed additional signal interferes with other signals to produce cross-modulation components. It can be seen from

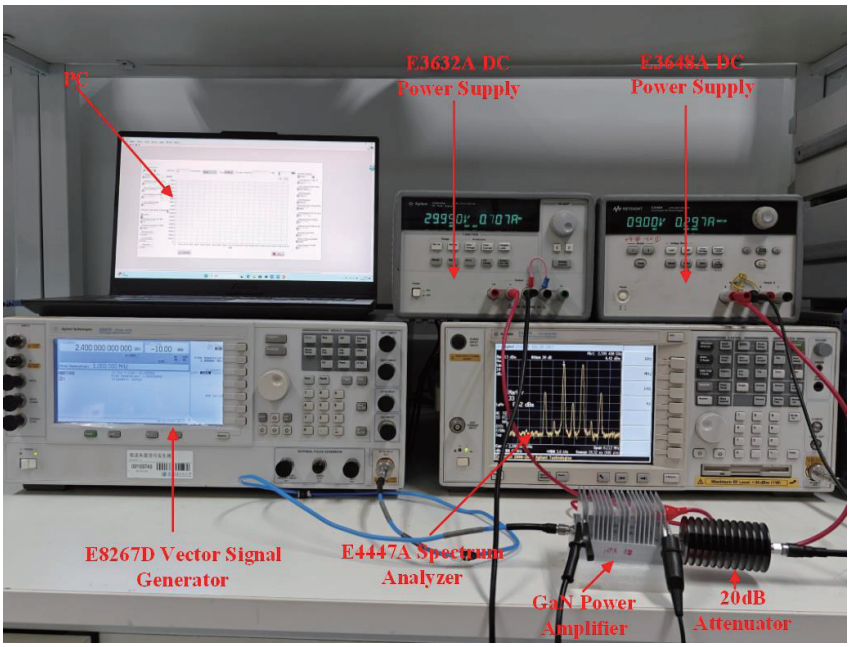

FIGURE 7. Measurement setup photograph including the LabVIEW control interface.

TABLE 2. Theoretical and experimental single-tone output comparison.

Parameters	Name	Theory	Measurement
Frequency (GHz)	f_0	2.4	2.40014
	$2f_0$	4.8	4.8001
	$3f_0$	7.2	7.20012
Output power (dBm)	$P_{out}(f_0)$	$Gain_{dB} + P_{in}(f_0) = 37.95$	37.31
	$P_{out}(2f_0)$	N/A*	11.61
	$P_{out}(3f_0)$		16.6
Voltage magnitude (mV)	A	7.07	6.99
	V_{o1}	558	518.8
	V_{o2}	N/A*	26.9
	V_{o3}		47.8

*N/A: Not applicable

Fig. 10(b) that at the same frequency, the gain of the fundamental wave and the output power of each component decrease with the increase of the input power.

5.2. GaN PA IMD3 Analysis Versus Input Power

During the present case of study, the VSG synthesizes TT signals with frequency interval $\Delta f_{12} = 10$ MHz. Then, the input signal powers $P_{out}(2f_1 - f_2)$ and $P_{out}(2f_2 - f_1)$ were increased linearly from $P_{in,\min} = -20$ dBm to $P_{in,\max} = 10$ dBm. The IM3 component power was recorded, and the corresponding characteristic representing IMD3 vs P_{in} is plotted in the left side of Fig. 10. Because of attenuation, the measured |IMD3| is slightly different from the theoretical calculation. When the input signal $P_{in} = 4$ dBm, the IM3 power reaches the maximum value. The third-order cross modulation distortion is the difference between the fundamental component and the cross-modulation component. As the input signal amplitude increases, the PA must operate in the NL region. Therefore, the third-order cross modulation increasing speed is greater than that of the fundamental component, and |IMD3| decreases. However, |IMD3| increases when the input signal is large, mainly because the cross-modulation component decreases.

5.3. PA NL Analysis Versus Carrier Frequency Interval

The characteristic plots of |IMD3| versus P_{out} at different interval frequencies $\Delta f_{12} =\{$ 100 kHz, 1 MHz, 10 MHz, 80 MHz$\}$ is shown in Fig. 11(a). It can be seen that |IMD3| at different interval frequencies can basically meet the requirements while the output power is the same. An interval frequency increase will result in a decrease of |IMD3|. Theoretically, as long as the conditions of equal amplitude and opposite phase are met,

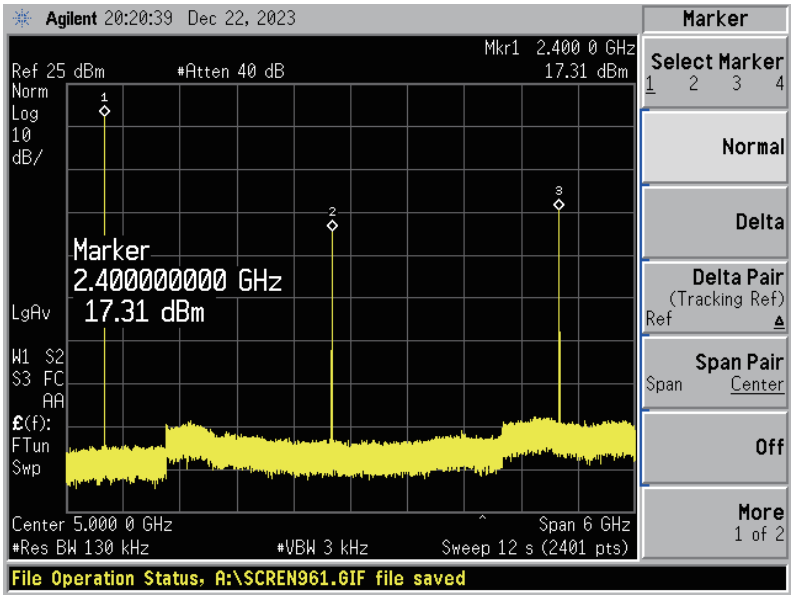

FIGURE 8. Output spectrum with f_0 single-carrier input.

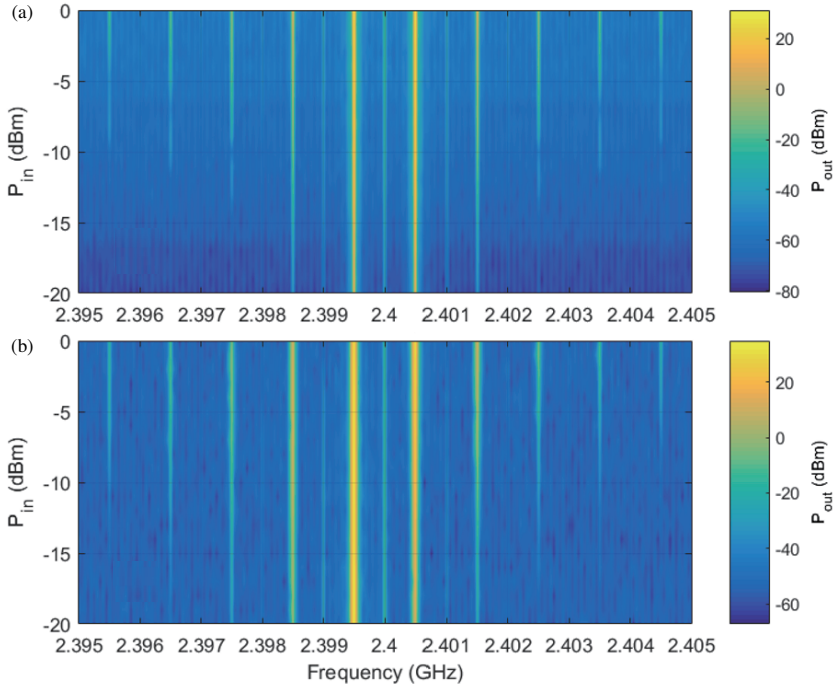

FIGURE 9. Mappings of measured PA output spectra with (a) same ($A_1 = A_2$) and (b) different ($A_1 \neq A_2$) input powers.

|IMD3| can be completely eliminated. However, in the actual experiment, there will be some third-order crossover distortion, because the amplitude cannot be exactly equal, and the phase is completely opposite. Therefore, with the increase of the TT signal interval frequency, the phase shift value of the signal changes. The phase shift value change leads to the reduction of the third-order crossover rejection. As the TT signal frequency interval becomes larger (from 100 kHz to 80 MHz), the suppression of |IMD3| decreases. This is because the frequency interval between the two branches of |IMD3| increases.

Due to the uneven frequency response of the instrument, it is more difficult for the two branches of third-order cross modulation distortion to meet the cancellation condition at the same time, resulting in the decrease of third-order cross modulation suppression degree. The characteristic plot of third-order cross-modulation rejection and frequency interval is shown in Fig. 11(b). When $P_{in} = -10$ dBm, the frequency interval is changed to obtain the signal output response. |IMD3| is calculated. When the frequency interval is varied between 8 MHz and 80 MHz, |IMD3| appears around degradation and asymme-

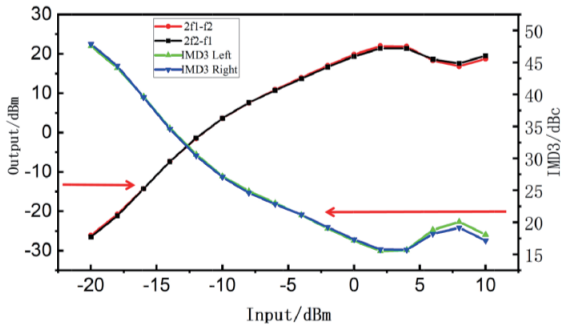

FIGURE 10. Measured IMD3 vs P_{in}.

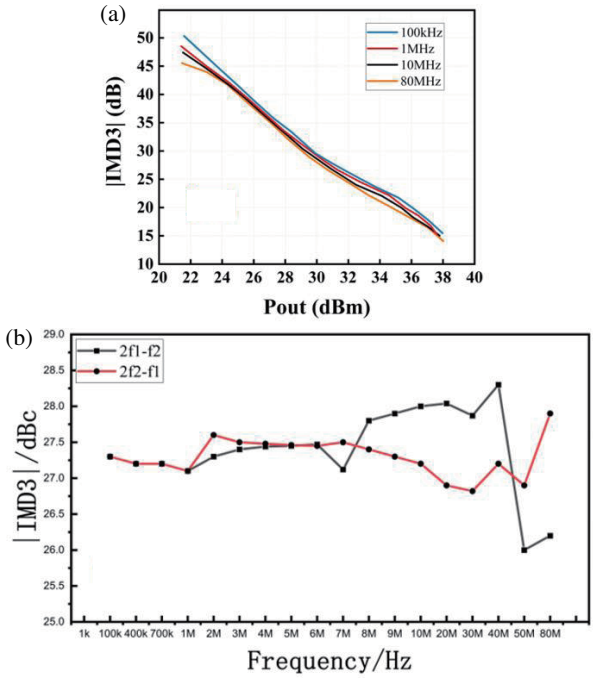

FIGURE 11. IMD3 versus (a) output power and versus (b) frequency interval.

try, and on behalf of the PA from interval frequency 8 MHz, memory effects begin to emerge. Based on memory effect analysis, when the input is assumed as DF signal, the PA output signal can be expressed in the function of two-carrier frequency interval. The PA output signal fundamental wave and each harmonic will also change accordingly. Therefore, the PA characteristic curve will also change, resulting in the phenomenon of upper and lower sideband imbalance, which produces a memory effect which (i) refers to the phenomenon that the NL DUT characteristics change with time. Meanwhile, the DUT current state is affected by its previous time [16, 19–21], (ii) reflects the phenomenon that under the PA same input power, and the gain, delay and other characteristics change at different times; (iii) memory effect is caused by the system internal components generally divided into three categories:

- Electrical memory effect: Inherent property of capacitance and inductance in the working circuit. Here, electrical memory effect is the main source of memory effect of PA.
- Electrothermal memory effect: Among them, the electric heating memory effect is related to the PA heat dissipation performance, and this effect can be avoided by achieving good heat dissipation.
- Semiconductor device notch effect [22–24]: It is related to the design and manufacturing process of the PA, and it is the characteristic of the PA itself. Mature manufacturing process can avoid this problem.

6. DF NL TEST WITH TT-INPUT SAME AND DIFFERENT AMPLITUDES

In this case, TT input signals with carrier frequencies $f_1 = 2.3995$ GHz and $f_2 = 2.4005$ GHz are injected into the PA. The input amplitude influence on PA NLT is discussed by using the developed DF method test bed in this section.

6.1. DF NL Test Results with Different Amplitude

Indeed, Table 3 summarizes the value of the IMD. Fig. 12 displays the PA output spectrum with non-equal-amplitude DF input signal ($P_{in}(f_1) = 0$ dBm, $P_{in}(f_2) = -10$ dBm). When $P_{in}(f_1) = 0$ dBm, $P_{in,min}(f_2) = -20$ dBm, and $P_{in,max}(f_2) = 0$ dBm, P_{out} and $|IMD3|$ vary in function of $P_{in}(f_2)$ as illustrated by Fig. 13(a) and Fig. 13(b), respectively.

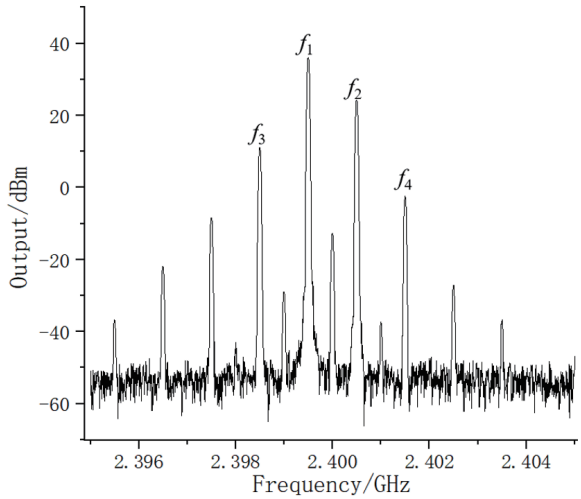

FIGURE 12. Output signal spectrum from DF NL test with different f_2 input ($P_{in}(f_1) = 0$ dBm, $P_{in}(f_2) = -10$ dBm).

TABLE 3. Comparison of calculated and measured IMD3 frequency values.

IMD3	Theory	Measurement
$2f_1f_2$	2398.5 MHz	2398.505 MHz
$2f_2f_1$	2401.5 MHz	2401.505 MHz

With the increase of $P_{in}(f_2)$, the output amplitude difference at the fundamental frequency becomes larger, because the components in the PA have a certain range of frequency response characteristics. The IMD3 theoretical model is based on Equation (6) based on PA output spectrum from single frequency

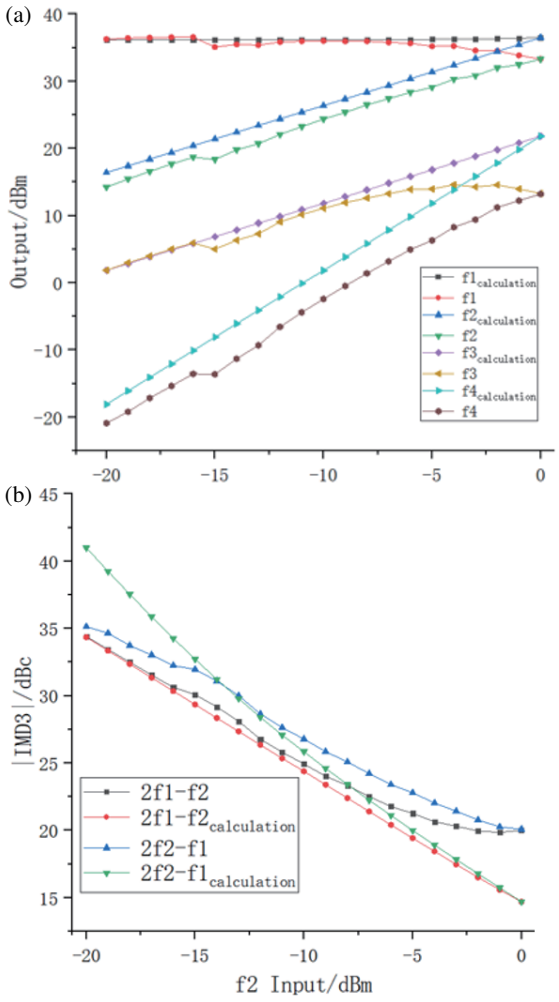

FIGURE 13. Comparison of tested and calculated (a) P_{out} and (b) |IMD3|.

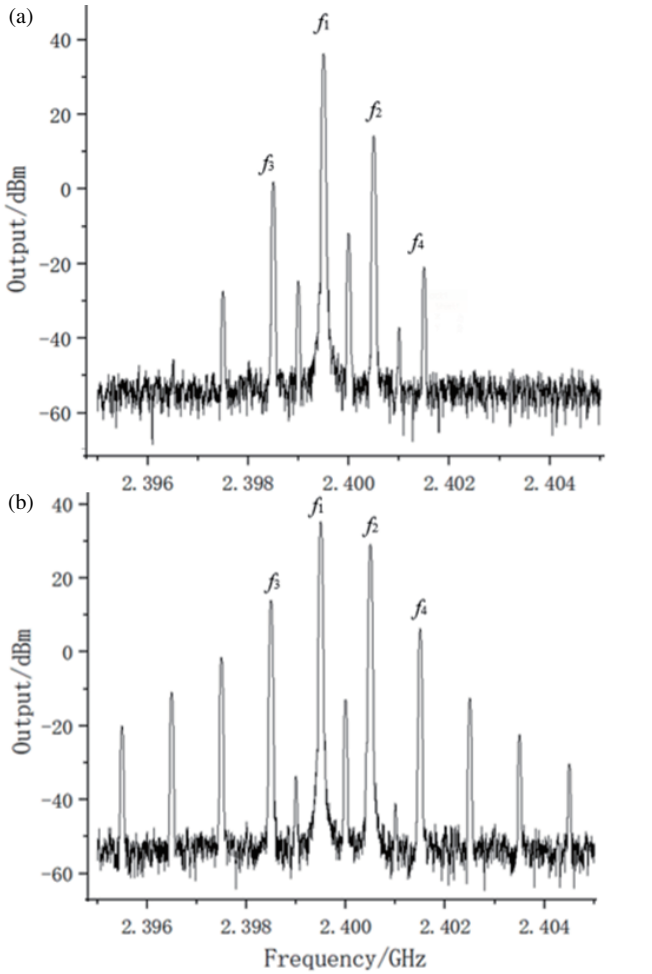

FIGURE 14. (a) Weak ($P_{in}(f_1) = 0$ dBm, $P_{in}(f_2) = -15$ dBm) and (b) strong ($P_{in}(f_1) = 0$ dBm, $P_{in}(f_2) = -5$ dBm) PA output responses.

spectrum plotted by Fig. 8. Fig. 13 confirms the good agreement between the measured and calculated IMD3. k_1 and k_3 corresponding to different input powers were determined from the TT input signal amplitudes. The theoretical amplitudes corresponding to f_1, f_2, f_3, and f_4 can be calculated. Fig. 13(a) compares the results from actual test amplitudes. It can be found that when $P_{in}(f_2)$ is less than -6 dBm, the difference between the calculated value and measured value does not exceed 2 dB, and the calculated and measured results are consistent with Equation (2) and highlight the PA weak NL stage. When $P_{in}(f_2)$ is more than -6 dBm, the difference between the calculated value and measured value gradually increases, and the gain of the power amplifier begins to compress. Fig. 13(b) compares the calculated value of IMD3 with the measured value. When $P_{in} < -16$ dBm, the calculated value of $P_{out}(2f_2 - f_1)$ is different from the measured value, because when the signal is very small, the error of the third-order intermodulation component read on the spectrum analyzer is large. With the increase of $P_{in}(f_2)$, the accurate value of the third-order intermodulation component can be obtained, and the calculated value of $P_{out}(2f_2 - f_1)$ is consistent with the measured value.

6.2. DF NL Test Results with Same Frequency Intervals

As shown in Fig. 14, as $P_{in}(f_2)$ increases, the PA behaves from weak to strong NLT which is manifested by the IMD3 reduction. When reaching the strong NL region, the PA responses include the IMD5 and higher-order IMD. Different rays can be identified from fundamental frequencies by linear combination. Since the DF signal and its interference components are theoretically symmetrical, the overall NL responses can be predicted by analyzing the data on the left side of the fundamental rays. It is foreseeable that with the input signal frequency increase, more linear combinations will appear. It implies that more interference components will also be generated. In more general analysis, even multiple interference components can be superposed at one frequency point. Thus, it can be emphasized that in a complex EM environment, the influence of multi-carrier input on the PA fundamental frequency is significant. As shown in Fig. 14, as $P_{in}(f_2)$ increases, the PA behaves from weak to strong NLT which is manifested by the IMD3 reduction. When reaching the strong NL region, the PA responses include the IMD5 and higher-order IMD. The different rays can be identified from fundamental frequencies by

TABLE 4. The difference between $2f_1 - f_2$ calculation results and measurements results.

$P_{in}(f_2)$/dBm	IMD3 calculation results/dBc	IMD3 measurement results/dBc
-18	38.17	34.96
-14	32.56	32.43
-8	25.14	26.37
-4	18.95	22.18
0	16.24	20.08

TABLE 5. Advantages of developed RF/microwave NL test method compared to existing ones.

Reference	Method	Contribution	Time cost	Operation	Amplitude non equal
[11]	Automatic DF measurement technique	DF test and identify intermodulation	-	DF	N
[21]	Multi-carrier amplitude phase test	Obtain multi-carrier phases	-	Multi-frequency	N
[22]	Load pulling measurement technology	Evaluate performance	-	Multi-frequency	N
[23]	Tri-frequency signal test	Analyze memory effects	-	Tri-frequency	N
[24]	Non-equal amplitude TT signal test		-	DF	Y
This paper	Automatic Double-multi-frequency test system	Analyze NLT and memory effects	5 minutes	Extend to Multi-frequency	Y

linear combination. Since the DF signal and its interference components are theoretically symmetrical, the overall NL responses can be predicted by analyzing the data on the left side of the fundamental rays. It is foreseeable that with the input signal frequency increase, more linear combinations will appear. It implies that more interference components will also be generated. In more general analysis, even multiple interference components can superpose at one frequency point.

Thus, it can be emphasized that in a complex EM environment, the influence of multi-carrier input on the PA fundamental frequency is significant.

6.3. Advantages of the Developed NL Test Bench

A state of the art on the comparison between the proposed work and other NL test research works of RF/microwave devices and systems is reported in this subsection. As shown in Table 4, the developed automatic test bench presents notable benefits. The automatic testing method is easy to operate and more user-friendly than manual testing. It can be emphasized that the automatic test system has advantages of cheap time cost, simple operation, possibility to consider different multi-tine amplitudes, and strong expansibility to higher order IMD characterization. It can also be used for multi-carrier testing. Compared with the traditional manual test [11, 21–24], the innovative system automatically injects signals to the tested part through the instrument control, saves and analyzes the output response data, improves the test efficiency, and enhances the stability. It can be used to analyze the impact of non-equal amplitude signals and memory effects on the system. In addition, the test bench can be potentially used for multi-carrier signal EMI analyses. The experimental results state the feasibility to use it for 5G and even future 6G active components, devices and communication systems.

7. CONCLUSION

An innovative automatic test bench of NL microwave device is developed based on the design of LabVIEW control interface. The automatic NL test bench integrates original multifunction interface as instrument control, data display, storage, and data processing. The effectiveness of the test bench is approved by a POC showing NL measurements of GaN PA operating around carrier frequency f_0.

The test results of DF TT signals with same and different amplitudes have important reference value for evaluating the EMI and environmental adaptability of the active component DUT. The GaN PA NL characteristics were quickly reported. The measured data can be exploited as well for setting subsequent NL modeling of RF/microwave components, devices and communication systems.

Compared to the existing NL measurement techniques [11, 19–22], the developed automatic test bench presents an outstanding efficiency. Indeed, the EMI analysis

from the developed automatic test bench with respect to the multi-frequency operation signals enables the evaluation of the communication quality with multi-carrier modulation in function of active component NLT.

In the future research, the systematic research of analyzing and measuring and solving the EMI induced NL characteristics of RF/microwave system as in 5G and 6G will be investigated.

ACKNOWLEDGEMENT

The research was carried out within the framework of joint project with the support of the National Key Research and Development Program of China (2022YFE0122700) and the Belarusian Republican Foundation for Fundamental Research (T22KITG-018).

REFERENCES

[1] Yaklaf, S. K. A., K. S. Tarmissi, and N. A. A. Shashoa, "6G mobile communications systems: Requirements, specifications, challenges, applications, and technologies," in *2021 IEEE 1st International Maghreb Meeting of the Conference on Sciences and Techniques of Automatic Control and Computer Engineering MI-STA*, 679–683, Tripoli, Libya, 2021.

[2] Wiklundh, K. and P. Stenumgaard, "EMC challenges for the era of massive Internet of things," *IEEE Electromagnetic Compatibility Magazine*, Vol. 8, No. 2, 65–74, 2019.

[3] Wiklundh, K. and P. Stenumgaard, "EMC challenges with 6G," in *2022 International Symposium on Electromagnetic Compatibility — EMC Europe*, 19–24, Gothenburg, Sweden, 2022.

[4] Mordachev, V., E. Sinkevich, Y. Yatskevich, A. Krachko, P. Zaharov, and X. Ma, "Simulation of nonlinear interference in aircraft systems operating in complex electromagnetic environment created by land-based and air-based wireless systems," in *2017 International Symposium on Electromagnetic Compatibility — EMC EUROPE*, 1–6, Angers, France, 2017.

[5] Abuelma'atti, M. T., "Analysis of the effect of radio frequency interference on the DC performance of bipolar operational amplifiers," *IEEE Transactions on Electromagnetic Compatibility*, Vol. 45, No. 2, 453–458, May 2003.

[6] Bayram, Y., J. L. Volakis, S. K. Myoung, S. J. Doo, and P. Roblin, "High-power EMI on RF amplifier and digital modulation schemes," *IEEE Transactions on Electromagnetic Compatibility*, Vol. 50, No. 4, 849–860, Nov. 2008.

[7] Refaie Ali, A., H. O. Roshid, S. Islam, and A. Khatun, "Analyzing bifurcation, stability, and wave solutions in nonlinear telecommunications models using transmission lines, Hamiltonian and Jacobian techniques," *Scientific Reports*, Vol. 14, No. 1, 15282, 2024.

[8] Fiori, F., "EMI-induced distortion of baseband signals in current feedback instrumentation amplifiers," *IEEE Transactions on Electromagnetic Compatibility*, Vol. 60, No. 3, 605–612, Jun. 2018.

[9] Fiori, F., "A new nonlinear model of EMI-induced distortion phenomena in feedback CMOS operational amplifiers," *IEEE Transactions on Electromagnetic Compatibility*, Vol. 44, No. 4, 495–502, Nov. 2002.

[10] Sinkevich, E. V., "Discrete nonlinear simulation of radio receivers for electromagnetic compatibility analysis and design: Estimation of the signal-to-interference ratio," in *2007 7th International Symposium on Electromagnetic Compatibility and Electromagnetic Ecology*, 166–169, St. Petersburg, Russia, 2007.

[11] Mordachev, V. I., "Automated double-frequency testing technique for mapping receive interference responses," *IEEE Transactions on Electromagnetic Compatibility*, Vol. 42, No. 2, 213–225, May 2000.

[12] Golubovich, D. and S. Chermoshentsev, "Virtual testing of the emission of electromagnetic interference from electronic means according to the electromagnetic compatibility requirements," in *2019 International Conference on Electrotechnical Complexes and Systems (ICOECS)*, 1–4, Ufa, Russia, 2019.

[13] Stelzried, C. T., "Non-linearity in measurement systems: Evaluation method and application to microwave radiometers," *The Telecommunications and Data Acquisition Report*, NASA, Nov. 1987.

[14] Pareschi, F., R. Rovatti, and G. Setti, "EMI reduction via spread spectrum in DC/DC converters: State of the art, optimization, and tradeoffs," *IEEE Access*, Vol. 3, 2857–2874, 2015.

[15] Yeh, M.-L., W.-R. Liou, H.-P. Hsieh, and Y.-J. Lin, "An electromagnetic interference (EMI) reduced high-efficiency switching power amplifier," *IEEE Transactions on Power Electronics*, Vol. 25, No. 3, 710–718, Mar. 2010.

[16] Auer, M. and T. Karaca, "Spread spectrum techniques for class-D audio amplifiers to reduce EMI," *E & I Elektrotechnik und Informationstechnik*, Vol. 133, No. 1, 43–47, 2016.

[17] Islam, S., B. Halder, and A. R. Ali, "Optical and rogue type soliton solutions of the (2 + 1) dimensional nonlinear heisenberg ferromagnetic spin chains equation," *Scientific Reports*, Vol. 13, No. 1, 9906, 2023.

[18] Refaie Ali, A., M. N. Alam, and M. W. Parven, "Unveiling optical soliton solutions and bifurcation analysis in the space–time fractional Fokas — Lenells equation via SSE approach," *Scientific Reports*, Vol. 14, No. 1, 2000, 2024.

[19] Xiao, Z. and X. Jing, "A novel characteristic parameter approach for analysis and design of linear components in nonlinear systems," *IEEE Transactions on Signal Processing*, Vol. 64, No. 10, 2528–2540, 2016.

[20] Celik, A., Z. Zhang, and P. P. Sotiriadis, "A state-space approach to intermodulation distortion estimation in fully balanced bandpass Gm-C filters with weak nonlinearities," *IEEE Transactions on Circuits and Systems I: Regular Papers*, Vol. 54, No. 4, 829–844, 2007.

[21] Martins, J. P. and N. B. Carvalho, "Multitone phase and amplitude measurement for nonlinear device characterization," *IEEE Transactions on Microwave Theory and Techniques*, Vol. 53, No. 6, 1982–1989, Jun. 2005.

[22] Gibiino, G. P., A. M. Angelotti, A. Santarelli, F. Filicori, and P. A. Traverso, "Multitone multiharmonic scattering parameters for the characterization of nonlinear networks," *IEEE Transactions on Instrumentation and Measurement*, Vol. 70, No. 2001612, 1–12, 2020.

[23] Ronnow, D., D. Wisell, and M. Isaksson, "Three-tone characterization of nonlinear memory effects in radio-frequency power amplifiers," *IEEE Transactions on Instrumentation and Measurement*, Vol. 56, No. 6, 2646–2657, Dec. 2007.

[24] Alizadeh, M. and D. Rönnow, "A two-tone test for characterizing nonlinear dynamic effects of radio frequency amplifiers in different amplitude regions," *Measurement*, Vol. 89, 273–279, 2016.

[25] Carvalho, N. B., K. A. Remley, D. Schreurs, and K. G. Gard, "Multisine signals for wireless system test and design," *IEEE Microwave Magazine*, Vol. 9, No. 3, 122–138, 2008.

[26] Sandberg, I. W. and G. J. J. V. Zyl, "Harmonic balance and almost periodic inputs," in *2002 IEEE International Symposium on Circuits and Systems. Proceedings (Cat. No.02CH37353)*,

Phoenix-Scottsdale, AZ, USA, May 2002.

[27] Minasian, R. A., "Intermodulation distortion analysis of MESFET amplifiers using the Volterra series representation," *IEEE Transactions on Microwave Theory and Techniques*, Vol. 28, No. 1, 1–8, 1980.

[28] Lima, E. G., T. R. Cunha, H. M. Teixeira, M. Pirola, and J. C. Pedro, "Base-band derived volterra series for power amplifier modeling," in *2009 IEEE MTT-S International Microwave Symposium Digest*, 1361–1364, Boston, MA, USA, Jun. 2009.

[29] Khan, M. H., S. Islam, and A. R. Ali, "Certain results associated with lump and periodic-soliton solutions for (2 + 1)-D Calogero–Bogoyavlenskii–Schiff equation," *Journal of Applied Mathematics and Statistical Analysis*, Vol. 4, No. 2, 43–57, 2023.

[30] Yang, X.-J., A. A. Alsolami, and A. R. Ali, "An even entire function of order one is a special solution for a classical wave equation in one-dimensional space," *Thermal Science*, Vol. 27, No. 1B, 491–495, 2023.

[31] Fu, K., C. L. Law, and T. T. Thein, "Test bed for power amplifier behavioral characterization and modeling," *Measurement*, Vol. 46, No. 8, 2735–2745, 2013.

[32] Panigrahi, S. R. and D. Rönnow, "Evaluating nonlinear distortion of single and dual channel excitation of an amplifier at 24 GHz," *Microwave and Optical Technology Letters*, Vol. 63, No. 9, 2315–2319, 2021.

[33] Horst, Van der M. J., A. C. Linnenbank, and A. van Staveren, "Amplitude-modulation detection in single-stage negative-feedback amplifiers due to interfering out-of-band signals," *IEEE Transactions on Electromagnetic Compatibility*, Vol. 47, No. 1, 34–44, Feb. 2005.

[34] Jin, C., M. T. Tan, and K. Y. See, "Filterless class-D amplifier with pseudorandomized carrier frequency modulation for EMI reduction," *IEEE Transactions on Electromagnetic Compatibility*, Vol. 55, No. 1, 74–80, Feb. 2013.

[35] Alizadeh, M., D. Rönnow, and P. Händel, "Characterization of Volterra kernels for RF power amplifiers using a two-tone signal and a large-signal," in *2018 International Conference on Communications (COMM)*, 351–356, Bucharest, Romania, 2018.

[36] Mordachev, V. and E. Sinkevich, "Experimental analysis of radio receiver susceptibility to out-of-band interference by means of double-frequency test system," in *10th International Symposium on Electromagnetic Compatibility*, 405–411, York, UK, 2011.

[37] Cheng, K.-K. M. and C.-F. Au-Yeung, "Novel difference-frequency dual-signal injection method for CMOS mixer linearization," *IEEE Microwave and Wireless Components Letters*, Vol. 14, No. 7, 358–360, Jul. 2004.